Malays. J. Anal. Sci. Volume 30 Number 5 (2026): 1908

MALAYSIAN JOURNAL OF ANALYTICAL SCIENCES

Journal homepage: https://mjas.analis.com.my/

Research Article

Synthesis of carbon quantum dots from disposable surgical masks for UV-induced apparent Eriochrome black T removal

Emerson De Los Reyes, Pauline Andres, Norelyn Arenas and Chelsea Allyssa Rayo, Rhonalyn Maulion*

Department of Chemical Engineering, College of Engineering, Batangas State University, The National Engineering University – Alangilan Batangas City, Batangas, 4200, Philippines

*Corresponding author: rhonalyn.maulion@g.batstate-u.edu.ph

Received: 16 April 2026; Revised: 10 July 2026; Accepted: 25 September 2026; Published: 31 October 2026

Abstract

The persistence of synthetic dyes in wastewater and the increasing accumulation of disposable surgical mask (DSM) waste represents concurrent environmental challenges that require sustainable solution through waste valorization strategies. Eriochrome Black T (EBT), an anionic azo dye, is of particular concern due to its chemical stability and resistance to biodegradation. Although carbon quantum dots (CQDs) have gained attention for environmental applications, limited studies have explored waste DSMs as carbon precursors for CQD synthesis and their application in apparent EBT removal. To address this gap, CQDs were synthesized from previously used DSMs via microwave-assisted method using ethylenediaminetetraacetic acid (EDTA) as a nitrogen-containing agent and evaluated for apparent EBT removal under UV irradiation. A face-centered central composite design was used to optimize synthesis conditions that yield a maximum photoluminescence (PL) intensity of 175.379 at 1 g DSM precursor, 630 W microwave power, and 15 min irradiation time. Analysis of variance at a 95% confidence level showed that DSM mass, microwave power, and irradiation time significantly affected the photoluminescence (PL) response. TEM analysis revealed an average particle size of 10.5 nm and a lattice fringe spacing of 0.316 nm. FTIR-ATR indicated surface functionalities potentially associated with O–H/N–H and C=C and/or C=N vibrations, while UV–Vis spectra exhibited π–π* and n–π* transitions. PL spectroscopy showed excitation and emission maxima at 363 and 461 nm respectively. The UV-induced apparent EBT removal performance was evaluated by varying initial EBT concentration, CQD suspension volume, and contact time. QCDs showed moderate UV induced EBT removal activity with 51.45% achieved after 5 hours of UV exposure. These findings suggest the potential of DSM-derived CQDs as value-added fluorescent nanomaterials for dye-removal applications.

Keywords: surgical mask carbon quantum dots, apparent EBT removal, microwave-assisted extraction, Eriochrome black T

Introduction

Water contamination is one of the key serious issues that the entire world is particularly concerned about. The United Nations estimates that 80% of wastewater is discharged into the environment without proper treatment which significantly contributes to the release of pollutants and toxins into water bodies [1]. One of the industries contributing significantly to untreated and unrecycled wastewater is textile manufacturing which accounts for about 17-20% of global industrial water pollution [2,3] which contains high levels of biochemical oxygen demand (BOD) and chemical oxygen demand (COD). One of the problematic dyes is EBT dye molecule, which is extensively utilized in cosmetics, textiles, pulp, food, leather, and plastic industries [4]. Due to their carcinogenic potential, nonbiodegradability, complicated chemical structure and high chemical stability, it is considered a high danger to wastewater quality [5]. EBT is an anionic azo dye used in the production of nylon and textile fabrics [6] with adverse effect on humans and animals [7]. The hazards posed by textile dyes are increasing due to their long-term accumulation and non-biodegradable nature that demands for the presence of efficient wastewater treatment. To address this issue, an easy, practical and affordable technique is the use of CQDs in degrading organic dye pollution. Microwave-assisted extraction which uses the carbonization of tiny organic molecules over a short reaction time can

be used to synthesize CQDs. Numerous researches investigate hybrids with CQDs like nitrogen might increase the morphological characteristics, electrical complexity, functionality and stability [8,9].

Nowadays, there is significant increase in the use of disposable surgical masks (DSM) as a preventative measure against the spread of the virus. While masks have been effective in reducing transmission, they have also led to a new form of pollution known as mask pollution. The surge in mask usage has led to an enormous number of disposable masks being used and improperly disposed of, resulting in a significant environmental issue. The disposal of these masks, often made from non-biodegradable materials, has raised concerns about the long-term impact on the environment, particularly in marine ecosystems [10]. DSMs consist of three layers: a soft, water-absorbent inner layer, a water-resistant outer layer made of nonwoven fibers, and a middle layer that acts as an antimicrobial filter mainly composed of amine- and amide-based nitrogenous compounds [11]. This study utilized DSMs as an active precursor and ethylenediaminetetraacetic acid (EDTA) as nitrogen functionalized carbon quantum dots (CQDs) and evaluate its performance on UV-induced apparent EBT removal.

Materials and Methods

In this study, three-ply used disposable surgical masks were used as a precursor material. All the reagents, including Eriochrome Black T (EBT, ≥99%), ethylenediaminetetraacetic-acid (EDTA, ≥99%), sodium hydroxide (NaOH, ≥98%) and sulfuric acid ($H_2SO_4, 95-98\%$) were of analytical reagent grade and were obtained from Sigma-Aldrich. All chemicals were used received without further purification.

Synthesis of CQDs:

Microwave-Assisted Extraction

The synthesis of CQDs involved acid-assisted carbonization of the previously used DSMs followed by microwave assisted extraction to produce QCDs. A schematic representation of the CQDs synthesis is presented in **Figure 1**. The DSMs were subjected to acid-assisted carbonization using 98% sulfuric acid (H_2SO_4). The masks were initially soaked in the acid for 6 hours followed by heating at 150 °C under continuous stirring for 3 hours. The resulting carbonized mixture was filtered and repeatedly washed with deionized water until a pH of approximately 6 was achieved. The obtained carbonized material was subsequently subjected to microwave-assisted treatment for CQD synthesis, facilitating rapid conversion of the carbonaceous precursor into nanoscale carbon structures within a short processing time [12].

The study employed a face-centered central composite design (FCCD) to optimize the synthesis of CQDs, as presented in Table 1. Three numerical factors were investigated: the mass of carbonized disposable surgical masks (DSMs), microwave power and irradiation time. The DSMs amount (0.5, 0.75, 1.0g) was added in 50mL of 0.1M EDTA solution which served as nitrogen precursor and diluted to 100mL with deionized water. The solution was irradiated for 5 to 15 minutes irradiation time using an Imarflex 23L microwave oven model MO-G23D at power of 350, 490 and 630W. The resulting mixture was initially filtered through Whatman Grade 42 filter paper to remove residual particulates and recover the CQD-containing filtrate. The filtrate was subsequently purified by dialysis using a 1000 Da molecular weight cut-off (MWCO) dialysis membrane for 24 hours to remove unreacted precursors, residual acids, salts and other low-molecular-weight impurities.

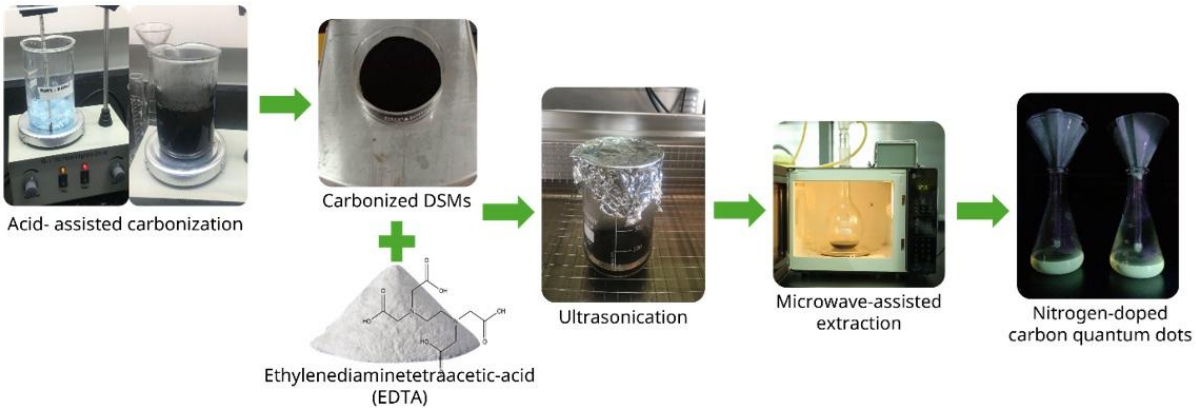


Figure 1. Preparation of carbon quantum dots

Table 1. Design of Experiment for the synthesis of carbon quantum dots

Factor	Unit	Low	Middle	High
Mass of DSM	g	0.5	0.75	1.0
Microwave power	W	350	490	630
Irradiation time	mins	5	10	15

Photoluminescence intensity metering set-up

Photos of the CQDs were taken using a digital single-lens reflex (DLSR) camera to capture light frequency, while the images were converted to a luminous intensity using Image J Batch Software [13]. A UV irradiation-chamber equipped with 365 nm UV lamp was prepared which serves as the DSLR-based fluorometer. An enclosed standard document instrument along with a good image capturing angle was considered to block background light. Relatively, appropriate eye protection was used as the UV light may pass through the chamber. The photoluminescence (PL) intensity of the sample was measured using the captured images processed through the RGB Measure plugin in ImageJ software [5].

Images were acquired using the camera's automatic exposure mode and positioned obliquely at 45° to reduce direct reflected excitation light at a constant distance of 10cm from the sample. The UV lamp (365 nm) was placed at a fixed distance of 15cm and angle of 90° relative to the sample to provide uniform excitation while the lamp-to-sample distance was maintained constant throughout the measurements. All images were captured under identical exposure and ambient-light conditions using a fixed experimental setup. Fluorescence intensity was analyzed using ImageJ by selecting a consistent region of interest (ROI) for all samples. Background intensity was measured from a blank or non-fluorescent region and subtracted from the sample intensity. The measurements were performed in triplicate with results reported as mean.

Characterization of N-QCDs

The TEM images were obtained using the JEOL JEM-2100F Field Emission Transmission Electron Microscope with accelerating voltage of 200kV. The generated images were used to establish particle size and distribution and lattice fringe spacing. FTIR-ATR was carried out using Agilent Cary 630 with 32 background scans in the range of 4000 cm^{-1} to 600 cm^{-1} with 4 cm^{-1} resolution. The adsorption spectra were scanned at 500 nm to 200 nm using UV-visible spectrophotometer. The data was used to establish the electronic transition and energy bandgap. The excitation and emission wavelength were analyzed using RF-5301 Spectro fluorophotometer with scan range from 220nm to 900nm, sample pitch of 1.0, slit width of 5.0 nm for both excitation and emission spectrum with super scan speed and high sensitivity.

Apparent EBT removal

The UV-induced apparent EBT removal was done in batch that used 10 mL of CQDs and diluted to 50 mL with dye concentration of 25ppm. The solution was exposed to UV-light irradiation at wavelength of 365 nm at a specified duration. The treated dye solutions were collected and analyzed using a UV-vis spectrophotometer. The percentage EBT dye degradation was calculated using (1)

$$\text{Percentage Removal (\%)} = \frac{C_0 - C_t}{C_0} \times 100\% \qquad (1)$$

where C_0 is the initial concentration of EBT dye and C_t is the concentration of EBT dye at time t. The absorbance value will be analyzed using UV-Vis spectrophotometer at a wavelength of 200-600 nm [14]. The effect of varying operating factors on the UV-induced apparent EBT removal was determined using a full factorial design. This study involved investigating three factors such as initial EBT dye concentration, volume of CQDs and contact time. The experimental design for three factors- three level full factorial is shown in **Table 2**.

Table 2. Design of Experiment for UV-induced Apparent EBT removal

Factor	Unit	Low	Middle	High
Dye concentration	ppm	25	50	75
Volume of CQDs	mL/50 mL	5	7.5	10
Contact time	hour	1	3	5

Results and Discussion

Characterization of carbonized disposable surgical masks

The carbonized disposable surgical masks (DSMs) were characterized using scanning electron microscopy coupled with energy-dispersive X-ray spectroscopy (SEM–EDS) to evaluate their surface morphology and elemental composition, particularly the presence and distribution of carbon and other detectable elements. The surface of the carbonized material from the surgical mask exhibits inhomogeneous morphology as observed in SEM micrographs (**Figures 2a and 2b**) using SE detector 10.0 kV. The observed clump where due to agglomeration of particles formed via acid carbonization. The elemental composition analysis presented in **Figures 2d and 2e** further indicates the potential of the material for carbon quantum dot synthesis. The observed clumps were due to agglomeration of particles formed via acid carbonization.

The analysis revealed the presence of three elements such carbon, oxygen, and sulfur respectively. Carbon accounts for the highest concentration at 69.5wt% followed by oxygen with 22.3 wt.%. Traces of sulfur were also observed corresponding to 8.2 wt.% which is attributed to the chemical carbonization of the precursor. The particle size distributions shown in **Figure 2c** follows a Gaussian distribution with an average particle size of 0.022 micrometers. The particle size obtained is attributed to the agglomeration of the carbonized materials which may occur due to weak van der Waals interactions between particles [15].

Effect of factors on synthesis of CQDs

Disposable surgical masks demonstrate promising potential as a carbon precursor for the synthesis of carbon quantum dots while the integration of nitrogen through ethylenediaminetetraacetic acid (EDTA) can further enhance their optical properties. The synthesis of CQDs was investigated and modeled to evaluate the effects of varying conditions such as mass of disposable surgical masks, microwave power, and irradiation time on their photoluminescence intensity (**Figure 3**) which was used as the response variable in the response surface analysis.

The response surface methodology results indicate that an increase in the mass of the carbon source leads to a corresponding increase in the photoluminescence intensity of the CQDs, as illustrated in Figure 3a. The mass of carbon precursors reported to have an evident positive impact on the photoluminescence of carbon quantum dots [16]. The increase in microwave power resulted in an increase in PL intensity which suggested that the increase in the microwave power is proportional to the increase in density of the moieties found on the surface of the carbon quantum dots which further results in the advantageous progress of the PL intensity [17].

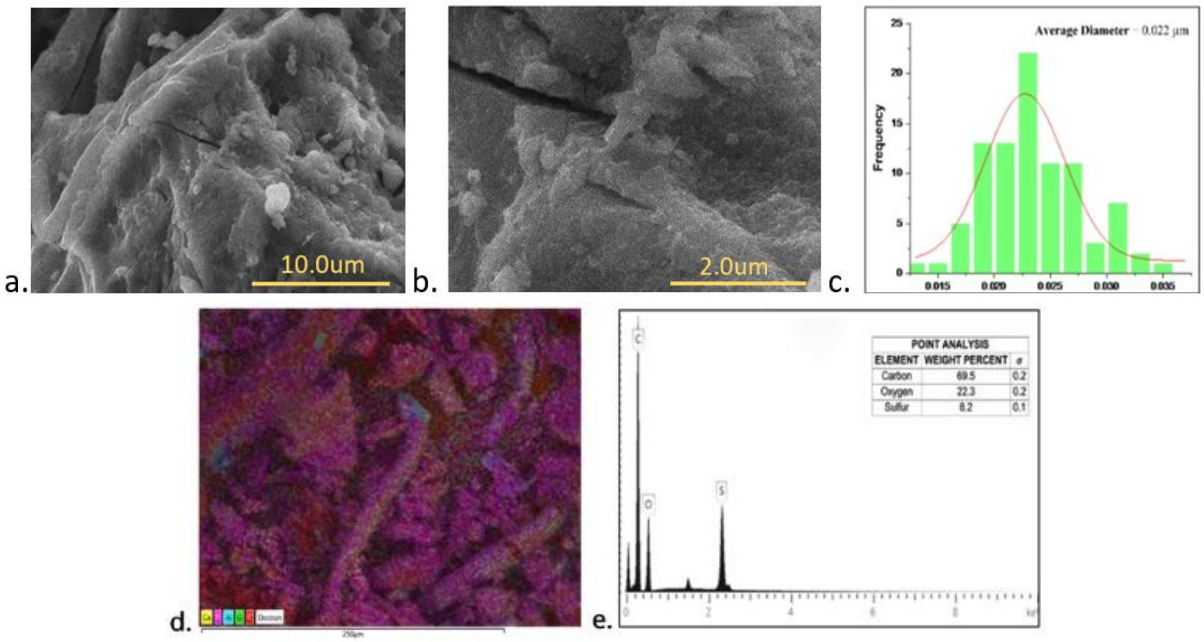


Figure 2. Surface morphology of carbonized DSMs (a) 5K magnification, (b) 20K magnification (c) Particle size and distribution of DSMs (d) EDS Mapping and (e) Percentage composition

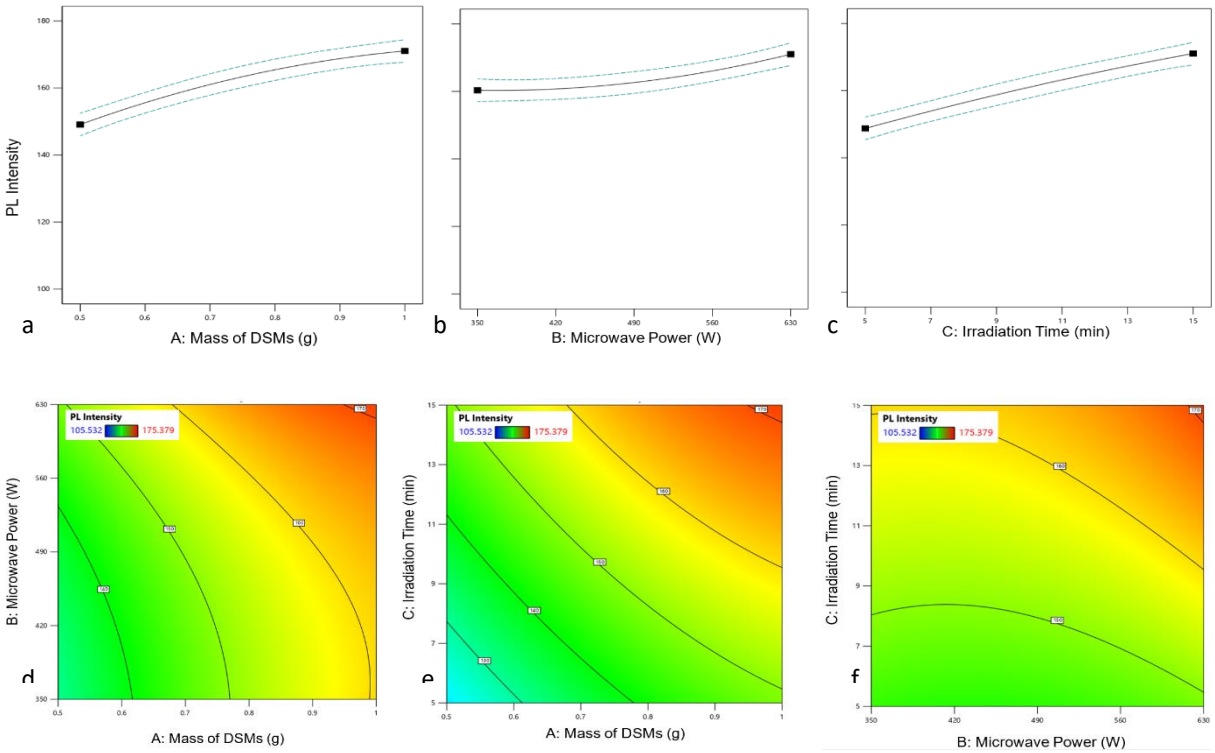


Figure 3. One-factor effect of (a) Mass of disposable surgical masks, (b) Microwave power, (c) irradiation time. Contour plot of (d) mass of DSMs and microwave power, (e) mass of DSMs and irradiation time, (f) microwave power and irradiation time

Consequently, irradiation time has a significant influence on PL intensity of the synthesized CQDs as shown in **Figure 3c** which indicates that the duration of irradiation directly affects the PL intensity of the sample. Longer reaction times promote a higher degree of carbonization that facilitates the formation of the carbon core and subsequently influences the optical properties of the carbon quantum dots [16].

Contour plots were generated to illustrate the interactions among the three significant factors The relationship between microwave power and the mass of disposable surgical masks (DSMs) and their influence on the PL intensity of CQDs is shown in **Figure 3d**. The color transition from green to red indicates an increase in PL intensity as both microwave power and DSM dosage increase. Figure 3e presents the combined effect of irradiation time and the dosage of carbonized disposable surgical masks where the color gradient shifts from blue to red with increasing irradiation time and precursor amount. Similarly, **Figure 3f** demonstrates the interaction between microwave power and irradiation time where the transition from green to red corresponds to an increase in PL intensity.

These observations suggest that prolonged heat exposure promotes the formation of more active quantum dots participating in photoexcitation [18] implying that sufficient energy input is required for quantum dot synthesis. However, excessively high microwave power leads to a decrease in PL intensity which indicates that the transformation of polymer-like CQDs into carbogenic CQDs were due to further carbonization of organic molecules in the sample [19]. The analysis of variance (ANOVA) indicated that the quadratic model provided a good fit with a p-value < 0.0001 and an F-value of 116.30 with R^2 value of 0.9567 that suggest strong predictive capability for new observations. The primary factors such as mass of disposable surgical masks, microwave power and irradiation time and their interactions significantly influenced the PL intensity at a significance level of 0.05 ($p < 0.0001$). Among these variables, the mass of disposable surgical masks exhibited the strongest effect as evidenced by the highest F-value of 578.04. Furthermore, the interaction between the mass of disposable surgical masks and microwave power was identified as the most significant among the interaction terms.

Characterization of nitrogen-doped carbon quantum dots

The characteristics of the synthesized nitrogen-doped carbon quantum dots were investigated using Transmission Electron Microscope (TEM), Fourier

Transform Infrared- Attenuated Total Reflection Spectroscopy (FTIR-ATR), UV-Visible Spectroscopy and Spectrofluorophometer to determine the morphology, particle size and distribution, functional groups, band gap and the excitation and emission spectrum of CQDs. The TEM micrographs in **Figure 4a** indicate that the CQDs in the sample are not well dispersed and aggregated, non-uniform spherical structures with low diffraction contrast. This observation may be attributed to the limited control over the size and shape of the carbon quantum dots during microwave irradiation [9, 18].

The inset HRTEM image in **Figure 4b** revealed discernible lattice fringes with an average interplanar spacing (d-spacing) of approximately 0.316 nm attributed to the presence of locally ordered carbon domains or graphitic or turbostratic carbon domains within the synthesized N-CQDs within the synthesized CQDs [20–22]. However, assignment of this d-spacing to a specific crystallographic plane was avoided in the absence of complementary XRD or SAED analysis. The Gaussian fitting curve shown in **Figure 4c** indicates a broad particle size distribution ranging from 4 to 22 nm with an average diameter of 10.5nm indicating the TEM observations that the CQDs exhibit non-uniform particle sizes and possible particle aggregation.

FTIR analysis in **Figure 5** revealed three major absorption features in different spectral regions. A broad band centered at approximately 3257cm^{-} may be attributed to overlapping O-H and N-H stretching vibrations which suggest the possible presence of nitrogen containing surface functional groups [24, 25]. The band observed approximately at 2107cm^{-1} may be related to unsaturated carbon functionalities whereas the absorption feature observed at 1636 cm^{-1} may be associated with C=C and/or C=N stretching vibrations in the carbonaceous structure [25, 26]. Similar absorption features associated with H/O-H stretching in the region around 3,400 cm^{-1} and C=C related vibrations near 1,600 cm^{-1} have been reported for carbon-based materials [27-28]. However, due to possible overlap among vibrational bands, these FTIR features provide only indirect evidence of nitrogen-containing surface functionalities and do not conclusively demonstrate nitrogen incorporation into the carbon framework.

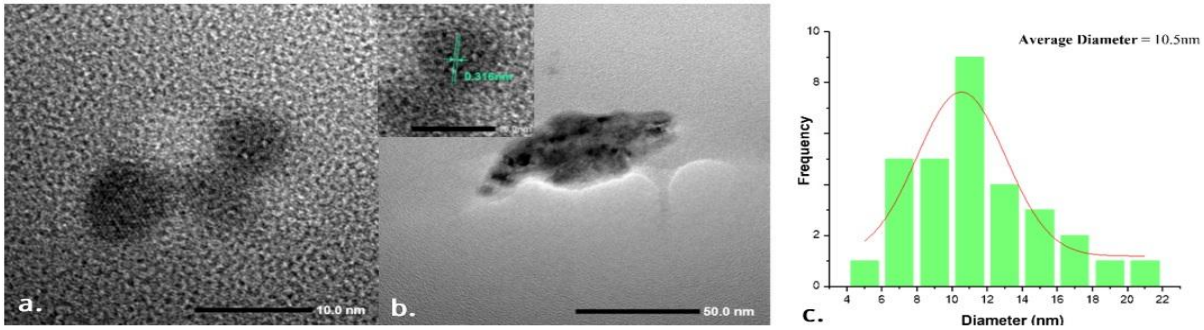


Figure 4. TEM images of the carbon quantum dots taken at (a) 850,000× and (b) 150,000×, with an inset showing the observed lattice fringes, and (c) particle size distribution

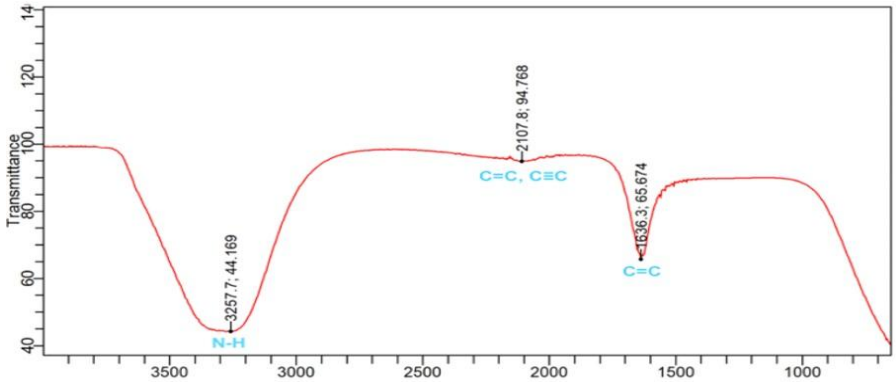


Figure 5. FTIR analysis of CQDs

The carbon molecules present in the graphene layers are replaced by the graphitic N atoms during doping [9]. Furthermore, the UV-vis spectra of the aqueous CQDs solution reveal two absorption bands as shown in the **Figure 6a**. The peak observed at 220 nm was assigned to the π-π* transition of the carbon atoms which captures excited-state energy through surface states. These outcomes provided evidence of unsaturated carbons in the carbon quantum dots. Moreover, peak detected at 300 nm in the absorption spectrum represents the n-π* transition which implies that the carbon quantum dots showed a robust optical absorption in the UV-visible spectrum presenting two distinct shoulders at 250 nm and 300 nm in the UV region and a prolonged tail in the visible region [20]. The band gap is the minimum required energy to excite an electron to a conduction band state where it can participate in conduction. The bandgap energy of the nitrogen-doped carbon quantum dots is 4.99 eV as shown in **Figure 6b**. The PL spectrofluorophotometer was used to evaluate the emission and excitation wavelength of the N-CQDs. The CQDs exhibited a m aximum excitation wavelength at approximately 363 nm and a maximum emission wavelength at approxim ately 461 nm, corresponding to blue fluorescence. Alt hough the CQD solution appeared greenish under UV illumination, the measured emission maximum was lo cated within the blue spectral region. The inset exhibits the N-CQD solutions under visible light (left) and UV light (right).

UV-induced apparent EBT removal using CQDs

The effect of various factors such as adsorbate concentration, volume of adsorbent and contact time on the photodegradation of EBT dye using the synthesized N-QCDs were investigated. The model's F-value of 63.34, p-value <0.0001 indicates its statistical significance. **Figure 7** shows the effect of main factors in the apparent EBT removal using CQDs.

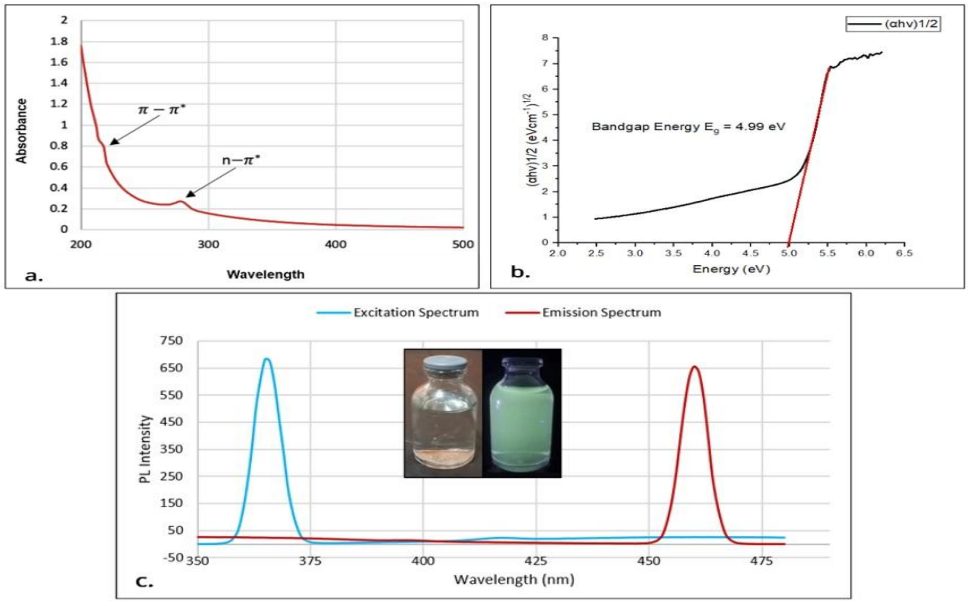


Figure 6. (a) Electronic transition, (b) Bandgap and (c) Fluorescence Spectrum of the Synthesized CQDs

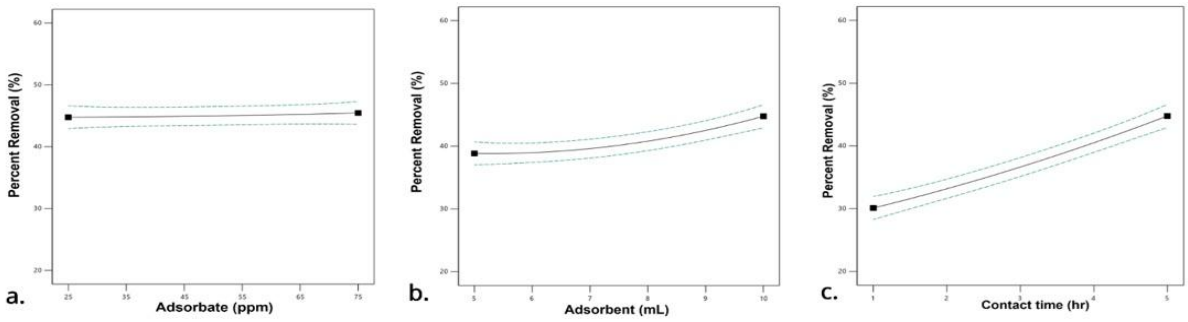


Figure 7. Effect-based influence of (**a**) adsorbate, (**b**) adsorbent and (**c**) contact time on the percentage degradation of EBT

Effect of EBT dye concentration

The effect of initial dye concentration on the UV-induced apparent removal of EBT was investigated over a concentration range of 25-75 ppm. The UV-induced apparent EBT removal efficiency exhibited only minimal variation across the studied concentration that indicate a limited influence of initial dye concentration under experimental conditions. Statistical analysis further showed that initial EBT concentration was not a significant within the studied range with a p-value of 0.0683 Consequently, at higher dye concentration, reduced removal efficiency maybe associated with increased light attenuation by dye molecules, which can limit photon availability for catalyst activation and consequently reduce the formation of reactive species [28]. Moreover, a fixed catalyst dosage may yield a limited number of reactive species which may not be adequate to counteract the effects of higher dye concentrations. Among the investigated conditions, 25 ppm exhibited the highest apparent EBT removal efficiency and was therefore identified as the best-performing initial concentration within the studied range. However, in the absence of photolysis and dark adsorption controls, the observed EBT removal cannot be attributed exclusively to UV-induced apparent EBT removal by the CQDs.

Effect of CQDs volume

The study involved an assessment of CQDs with a volume ranging from 5 mL to 10 mL and the analysis yielded a *p*-value <0.0001, which indicates that the volume of CQDs is a significant factor. Figure 7b illustrates the effect of dose on percept uptake of EBT onto NCQDs indicates rapid increase in degradation with increasing doses [29]. With 5 and 10 mL of NCQDs, EBT removal increased from 11.1 to 51.45%. A volume of 10 mL of CQDs can produce an adequate number of active sites that can result in increased radical generation. However, it should be observed that exceeding this amount may lead to an increase in turbidity within the mixture due to the presence of NCQDs. This heightened turbidity may hinder UV-light penetration, which can result in decreased efficiency in particle surface degradation. Thus, 10 mL was selected as the best volume condition.

Effect of contact time

The effect of contact time on the UV-induced apparent EBT removal using the synthesized carbon quantum dots was evaluated by adjusting contact time from 1 hour to 3 hours and 5 hours (**Figure 7c**). A distinct change in the hue of the dye upon the introduction of CQDs, indicating active photocatalytic interaction. Statistical analysis confirmed that contact time was highly significant parameter with a *p*-value of less than 0.0001 (**Table 5**). Contact in addition to the volume improved the system's optimum condition. With increasing contact time, a decrease in the reaction rate occurs following first-order kinetics, leading to competition between reactant and intermediate products during the degradation process. Two reasons account for the observed decline in kinetics beyond the optimal level: (i) the presence of short-chain aliphatic molecules alongside hydroxyl radicals that impede reaction progression, and (ii) the photocatalyst's short lifespan due to the deposition of potent by-products that cause deactivation of active sites [30]. When the contact time is increased, dye absorption increases dramatically. This is due to the interaction of EBT dye and surface of the nitrogen-doped carbon quantum dots. As the contact time increases, the interaction between the EBT dye and CQDs also increases resulting in the increase in photodegradation efficiency. Therefore, 5 hours was considered to be the best time for the EBT dye degradation onto the synthesized nitrogen-doped carbon quantum dots.

Time dependent removal of EBT

The time-dependent removal of EBT by the CQDs was evaluated using pseudo-first-order, pseudo-second-order and intraparticle diffusion kinetic models. These models were applied to describe the apparent EBT removal behavior under the investigated conditions. Because dark adsorption and UV-only controls were not conducted, the fitted kinetic parameters represent the overall removal process and cannot distinguish among adsorption, photolysis, and photocatalytic degradation. Presented in Figure 8 the pseudo-first-order, pseudo-second-order and intraparticle diffusion kinetic models of EBT dye removal.

The results showed that the pseudo-second-order kinetic model provided the best fit to the experimental data, with an R^2 value of 0.9954 and a fitted rate constant of 0.00267 [appropriate unit] with 1st order ($R^2 = 0.9172$) and intraparticle diffusion (1st order ($R^2 = 0.922$). This finding indicates that the pseudo-second-order model adequately describes the apparent EBT removal behavior under the investigated conditions. However, the good fit of this model should not be interpreted as definitive evidence of chemisorption or a specific chemical reaction between EBT and the surface functional groups of the CQDs. Given the absence of dark adsorption and UV-only photolysis controls, the observed EBT removal may involve combined contributions from adsorption, photolysis, and other UV-induced processes.

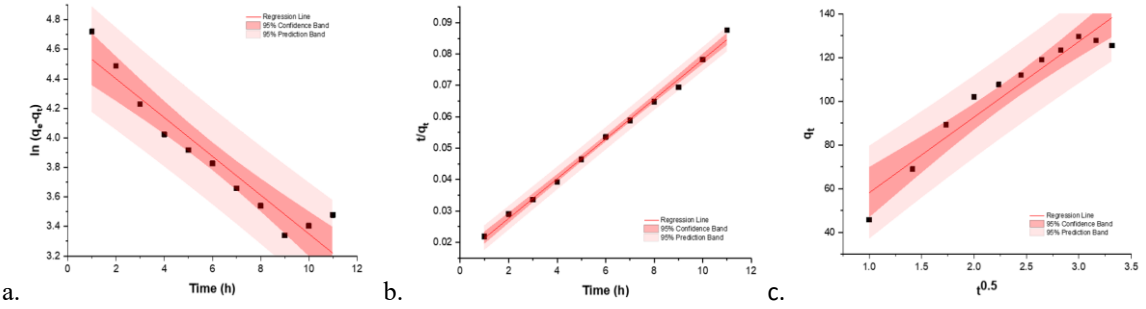


Figure 8. (a) Pseudo first order, (b) Pseudo second order and (c) intraparticle diffusion kinetic model of EBT removal

Table 3. Comparison of rate constants of reported studies

Adsorbent	Dye	Light	k_2 PSO Kinetic Model	Reference
CQDs from Disposable Surgical Masks (DSM)	EBT	Ultraviolet	0.0026	This study
N-CQDs from Empty fruit bunches (EFB)	EBT	Ultraviolet	Not specified	[30]
ZnSe quantum dot nanocomposite hydrogel (ZnSe QD-NCH)	CV	Ultraviolet	0.0021	[31]
B/P-CQDs	MB	Visible Light	0.891	[32]

EBT- Eriochrome Black T, CV-Crystal Violet, MB- Methylene Blue

The following table presents selected studies for comparison with the present findings. It summarizes different types of carbon quantum dots investigated for dye-removal applications, together with the kinetic models used and their corresponding fitted rate constants. Attention is given to studies reporting pseudo-second-order kinetic behavior to facilitate comparison with the apparent EBT removal observed in the present study.

Comparison with previous studies reveals both similarities and differences. The N-CQDs derived from empty fruit bunches (EFB) [30] were likewise reported for EBT removal under ultraviolet irradiation directly comparable study in terms of dye type, carbon quantum dot-based material and irradiation source. However, the reported comparison does not specify a k_2 value, preventing a quantitative assessment of the relative apparent removal rates. Nevertheless, the use of N-CQDs for the same EBT target supports the applicability of heteroatom-containing CQD materials in UV-assisted dye removal systems. The present study also exhibited a fitted k_2 value comparable to that reported for the ZnSe quantum dot nanocomposite hydrogel (ZnSe QD-NCH) used for Crystal Violet removal under UV irradiation. The ZnSe QD-NCH system showed a k_2 value of 0.0021 while the present DSM-derived CQDs exhibited a slightly higher value of 0.00267. Numerically, the fitted rate constant of the present study is approximately 27% higher than that of the ZnSe QD-NCH system) [31] which suggests faster apparent PSO kinetics under the respective experimental conditions. However, this comparison should be interpreted cautiously because the two studies differ in the target dye, material composition, surface properties, initial dye concentration, catalyst or adsorbent dosage, solution chemistry and irradiation conditions. Thus, the higher k_2 value cannot by itself establish superior intrinsic performance of the DSM-derived CQDs.

In contrast, the B/P-CQDs used for Methylene Blue removal under visible-light irradiation exhibited a much larger reported k_2 value of 0.891 which is approximately 334 times greater than the fitted value of 0.00267 obtained in the present study. This substantial difference may reflect variations in CQD composition and heteroatom doping, dye molecular structure and charge, light source, experimental conditions and the units or formulation used to report the PSO rate constant. Therefore, direct numerical comparison of k_2 values across these studies should be made only when the kinetic equations, units, and experimental conditions are consistent.

Proposed EBT removal pathways under UV irradiation

The UV–Vis spectrum of the aqueous CQD dispersion exhibited an absorption band at approximately 220 nm (**Figure 6a**), which is commonly associated with π–π* transitions of C=C bonds within sp^2-conjugated carbon domains. This observation suggests the

presence of conjugated carbon structures that may contribute to the optical response of the synthesized N-CQDs. Nitrogen incorporation and surface functional groups may further modify the electronic and surface states of the N-CQDs that may influence their photoresponse and interfacial interactions with EBT. However, the specific nitrogen configurations cannot be established in the absence of complementary chemical-state analysis such as XPS.

Under UV irradiation, photoexcited states of the CQDs may participate in electron-transfer processes involving dissolved oxygen and water and will potentially contribute to the formation of reactive oxygen species (ROS), such as superoxide ($O_2^{\bullet-}$) and hydroxyl (•OH) radicals. If generated, these reactive species may contribute to the transformation or partial degradation of EBT. In parallel, oxygen- and nitrogen-containing surface functional groups may facilitate interactions with EBT while π–π interactions between the conjugated carbon domains of the N-CQDs and the aromatic structure of EBT may also contribute to the observed removal behavior. These possible pathways are consistent with literature-reported mechanisms for CQD-based UV-induced dye removal.

However, these pathways remain proposed rather than experimentally confirmed mechanisms. Although the pseudo-second-order kinetic model provided the best fit to the experimental data (R^2 = 0.9954),compared with the first-order (R^2 = 0.9172) and intraparticle diffusion (R^2 = 0.922) models, this empirical fit does not independently establish chemisorption or a specific photocatalytic pathway. In the absence of radical scavenger tests, dark adsorption controls, UV-only photolysis controls and mineralization analyses, the observed 51.45% EBT removal after 5 hours cannot be attributed exclusively to photocatalytic degradation. Therefore, the results are conservatively interpreted as moderate UV-induced EBT removal, potentially arising from combined contributions of surface interactions, direct photolysis, and other N-CQD-assisted UV-induced processes.

Conclusion

This study utilized previously used disposable surgical masks (DSMs) as a carbon precursor for the synthesis of carbon quantum dots (CQDs) via acid-assisted carbonization followed by microwave-assisted treatment. The investigated synthesis parameters particularly DSM mass, microwave power and irradiation time, significantly influenced the photoluminescence response of the CQDs. FTIR analysis indicated the presence of surface functional groups associated with O–H/N–H and C=C and/or C=N vibrations; however, these findings provide only indirect evidence of nitrogen-containing functionalities and do not conclusively confirm nitrogen doping. The synthesized CQDs exhibited an average particle size of 10.5 nm and blue fluorescence with a maximum emission wavelength of approximately 461 nm. Under the investigated conditions, the CQDs achieved a maximum apparent EBT removal of 51.45% after 5 hours of UV exposure. However, due to the absence of dark adsorption, UV-only photolysis and appropriate catalyst control experiments, the observed EBT removal cannot be attributed exclusively to photocatalytic degradation. Overall, the findings demonstrate the potential of converting used DSM waste into value-added fluorescent carbon nanomaterials for environmental applications. Future studies should incorporate appropriate control experiments, degradation kinetics, radical scavenger studies, reusability assessments, mineralization analyses and complementary elemental characterization such as XPS or CHNS to clarify the removal mechanism and verify nitrogen incorporation.

Acknowledgement

The authors acknowledge the research support provided by the Chemical Engineering laboratory of Batangas State University – The National Engineering University. Analytical Services of NASAT Labs, Philippines, Department of Science and Technology-Material Science Division, University of the Philippines Los Banos, Laguna, and De La Salle University – Laguna Philippines for the nanoparticle analysis and characterization.

References

1. UNESCO World Water Assessment Programme (2024). The United Nations World Water Development Report 2024: Water for Prosperity and Peace. Access from https://www.unwater.org/publications/un-world-water-development-report-2024. [Access online 24 March 2026].
2. Islam, M. M., Rahman, M. M., and Hasan, M. T. (2025). A critical review on textile dye-containing wastewater: Ecotoxicity, health risks and remediation strategies for environmental safety. *Cleaner Chemical Engineering*, 11: 100165.
3. Singh, B. J., Kumar, P. and Sharma, R. (2023). A systematic review of industrial wastewater management: Evaluating challenges and enablers. *Journal of Environmental Management,* 348: 119230.
4. Çetinkaya, H. F., Aydin, S. and Yilmaz, A. (2025). Biosorptive removal of textile dye Eriochrome Black T from aqueous solution. *Journal of Molecular Liquids,* 408: 125015.
5. Lellis, B., Fávaro-Polonio, C. Z., Pamphile, J. A.,

& Polonio, J. C. (2019). Effects of textile dyes on health and the environment and bioremediation potential of living organisms. *Biotechnology Research and Innovation,* 3(2), 275–290.

6. Chatla, A., Almanassra, I. W., Kochkodan, V., Laoui, T., Alawadhi, H., & Atieh, M. A. (2022). Efficient removal of eriochrome black T (EBT) dye and chromium (CR) by hydrotalcite-derived MG-CA-AL mixed metal oxide composite. *Catalysts,* 12(10), 1247.
7. Slama, H. B., Bouket, A. C., Pourhassan, Z., Alenezi, F. N., Silini, A., Cherif-Silini, H., et al. (2021). Diversity of synthetic dyes from textile industries, discharge impacts and treatment methods. *Applied Sciences,* 11(14), 6255.
8. Yalshetti, S., Patil, A., Patil, S. and Gasti, T. (2024). Microwave-assisted synthesis, characterization and biomedical applications of carbon quantum dots: A review. *Nanomaterials,* 14 (5): 420 – 436.
9. Shaik, S. A., Sengupta, S., Varma, R. S., Gawande, M. B., & Goswami, A. (2020). Syntheses of N-doped carbon quantum dots (NCQDs) from bioderived precursors: A timely update. *ACS Sustainable Chemistry & Engineering,* 9(1), 3–49.
10. Aragaw, T. A. (2020). Surgical face masks as a potential source for microplastic pollution in the COVID-19 scenario. *Marine Pollution Bulletin,* 159: 111517.
11. Bumajdad, A., & Khan, M. J. H. (2021). The reuse of disposable COVID-19 surgical masks as a nitrogen-enrichment agent and structure promotor for a wild plant-derived sorbent. *Journal of Industrial and Engineering Chemistry*, 102, 163–176
12. Xu, Q., Kuang, T., Liu, Y., Cai, L., Peng, X., Sreeprasad, T. S., et al. (2016). Heteroatom-doped carbon dots: synthesis, characterization, properties, photoluminescence mechanism and biological applications. *Journal of Materials Chemistry B*, *4*(45), 7204–7219
13. Canson, M., Cantos, J., & de Guzman, M. (2016). Modelling the effect of varying Cr^{+6} and Cu^{+2} concentration on the luminous intensity of photobacterium phosphoreum in simulated seawater. Thesis Bachelor of Chemical Engineering.
14. Najjar, M., Nasseri, M. A., Allahresani, A., & Darroudi, M. (2022). Green and efficient synthesis of carbon quantum dots from *Cordia myxa L*. and their application in photocatalytic degradation of organic dyes. *Journal of Molecular Structure*, 1266, 133456.
15. Kausar, A. (2022). *Polymeric Nanocomposites with Carbonaceous Nanofillers for Aerospace Applications*. Elsevier.
16. Anuar, N. K. K., Tan, H. L., Lim, Y. P., So'aib, M. S., & Bakar, N. F. A. (2021). A review on Multifunctional carbon-dots synthesized from biomass waste: design/ fabrication, characterization and applications. *Frontiers in Energy Research*, 9, 626549.
17. Farsi, B. A., Sofin, R. G. S., Shidhani, H. A., El-Shafey, E.-S. I., Al-Hosni, A. S., Marzouqi, F. A., et al. (2022). The effect of microwave power level and post-synthesis annealing treatment on oxygen-based functional groups present on carbon quantum dots. *Journal of Luminescence*, *252*, 119326.
18. Ghanem, A., Al-Marjeh, R. A.-Q. B., & Atassi, Y. (2020). Novel nitrogen-doped carbon dots prepared under microwave-irradiation for highly sensitive detection of mercury ions. *Heliyon*, *6*(4), e03750.
19. Song, Z., Chen, X., Gong, X., Gao, X., Dai, Q., Nguyen, T. T., & Guo, M. (2020). Luminescent carbon quantum dots/nanofibrillated cellulose composite aerogel for monitoring adsorption of heavy metal ions in water. *Optical Materials*, 100, 109642.
20. Dela Cruz, Ma. I. S., Thongsai, N., De Luna, M. D. G., In, I., & Paoprasert, P. (2019). Preparation of highly photoluminescent carbon dots from polyurethane: Optimization using response surface methodology and selective detection of silver (I) ion. *Colloids and Surfaces a Physicochemical and Engineering Aspects*, 568, 184–194.
21. Mondal, T. K., Dinda, D., & Saha, S. K. (2018). Nitrogen, sulphur co-doped graphene quantum dot: An excellent sensor for nitroexplosives. *Sensors and Actuators B Chemical*, 257, 586–593.
22. Wang, R., Wang, X., & Sun, Y. (2016). One-step synthesis of self-doped carbon dots with highly photoluminescence as multifunctional biosensors for detection of iron ions and pH. *Sensors and Actuators B Chemical*, *2*41, 73–79
23. Singh, A., Qu, Z., Sharma, A., Singh, M., Tse, B., Ostrikov, K., et al. (2022). Ultra-bright green carbon dots with excitation-independent fluorescence for bioimaging. *Journal of Nanostructure in Chemistry*, 13(3), 377–387.
24. Ozyurt, D., Kobaisi, M. A., Hocking, R. K., & F ox, B. (2023). Properties, synthesis, and applicat ions of carbon dots: A review. *Carbon Trends,* 12, 100276.
25. Nguyen, K. G., Baragau, I. A., Gromicova, R., N icolaev, A., Thomson, S. A., Rennie, A., ... & K ellici, S. (2022). Investigating the effect of N-do ping on carbon quantum dots structure, optical p roperties and metal ion screening. *Scientific Reports*, 12(1), 13806.
26. Lazar, P., Mach, R., & Otyepka, M. (2019).

Spectroscopic fingerprints of graphitic, pyrrolic, pyridinic, and chemisorbed nitrogen in N-doped graphene. *The Journal of Physical Chemistry C*, 123(16), 10695-10702.

27. Patir, K., & Gogoi, S. K. (2018). Nitrogen-doped carbon dots as fluorescence ON–OFF–ON sensor for parallel detection of copper(II) and mercury(II) ions in solutions as well as in filter paper-based microfluidic device. *Nanoscale Advances*, *1*(2), 592–601.
28. Zaib, M., Akhtar, A., Maqsood, F., & Shahzadi, T. (2021). Green synthesis of carbon dots and their application as photocatalyst in dye degradation studies. *Arabian Journal for Science and Engineering*, 46(1), 437-446.
29. Abd Rani, U., Ng, L. Y., Ng, C. Y., Mahmoudi, E., Ng, Y. S., & Mohammad, A. W. (2021). Sustainable production of nitrogen-doped carbon quantum dots for photocatalytic degradation of methylene blue and malachite green. *Journal of Water Process Engineering*, 40, 101816.
30. Karim, S., Ahmad, N., Hussain, D., Mok, Y. S., & Siddiqui, G. U. (2022). Active removal of anionic azo dyes (MO, CR, EBT) from aqueous solution by potential adsorptive capacity of zinc oxide quantum dots. *Journal of Chemical Technology & Biotechnology*, *97*(8), 2087-2097.
31. Abdolahi, G., Dargahi, M., & Ghasemzadeh, H. (2020). Synthesis of starch-g-poly(acrylic acid)/ZnSe quantum dot nanocomposite hydrogel, for effective dye adsorption and photocatalytic degradation: thermodynamic and kinetic studies. *Cellulose, 27*(11), 6467–6483.
32. Yadav, S., Kumar, A., & Kumar, D. (2023). Photo degradation of methylene blue onto Boron/Phosphorous modified carbons dots prepared by hydrothermal and microwave assisted methods. *Materials Science for Energy Technologies*, *6*, 260-266.